npj | climate and atmospheric science

Article

Published in partnership with CECCR at King Abdulaziz University

https://doi.org/10.1038/s41612-024-00767-2

A hybrid approach for skillful multiseasonal prediction of winter North Pacific blocking

Mingyu Park [1,2] ✉, Nathaniel C. Johnson [2], Jaeyoung Hwang [3,4] & Liwei Jia [2]

Wintertime atmospheric blocking often brings adverse environmental and socioeconomic impacts through its accompanying temperature and precipitation extremes. However, due to the chaotic nature of the extratropical atmospheric circulation and the challenges in simulating blocking, the skillful seasonal prediction of blocking remains elusive. In this study, we leverage both observational data and seasonal hindcasts from a state-of-the-art seasonal prediction system to investigate the prediction skill of North Pacific wintertime blocking frequency and its linkage to downstream cold extremes. The observational results show that North Pacific blocking has a local maximum over the central North Pacific Ocean and that the occurrence of North Pacific blocking drives significant cold anomalies over northwestern North America within a week, which are both well reproduced by the model. The model skillfully predicts the western North Pacific blocking frequency near the subtropical jet exit region at the shortest forecast lead, but skill drops off rapidly with lead time partly due to model drift in the background flow. To overcome this rapid drop in skill, we develop a linear hybrid dynamical-statistical model that uses the forecasted Niño 3.4 index and upstream precipitation as predictors and that maintains significant forecast skill of high-latitude North Pacific blocking up to 7 lead months in advance. Our results indicate that an improvement in the seasonal prediction skill of winter North Pacific blocking frequency may be achieved by the enhanced representation of the links among sea surface temperature anomalies, tropical convection, and the ensuing tropical-extratropical interaction that initiates North Pacific blocking.

Atmospheric blocking is characterized by persistent and quasi-stationary high-pressure systems that frequently develop in the mid-to-high latitudes, particularly near the exit of the Pacific and Atlantic jet streams. The evolution of blocking involves a persistent meandering of the jet stream, which disrupts the midlatitude westerly flow and propagation of synoptic-scale systems[1,2]. This disruption of regional atmospheric circulation, if sustained for a week or longer, can lead to extreme weather events that pose significant socioeconomic risks[3]. For instance, during boreal winter, blocking exerts a significant downstream impact on the occurrence of cold extremes over many different regions, including East Asia[4,5], Eurasia[6], North America[7–9], and Europe[10–12]. This blocking-extreme weather linkage in turn emphasizes the need for accurate prediction of blocking in operational forecasts since blocking occurrence can serve as a source of predictability for extreme weather events on a regional scale[13,14].

The prediction of atmospheric blocking has been frequently noted as a long-standing challenge in current weather prediction systems. This difficulty partly originates from the chaotic nature of the extratropical atmospheric circulation that makes blocking onset difficult to predict[15,16] and from the incomplete understanding of the blocking dynamics due to its complexity[2,13]. Imperfect modeling systems with systematic biases in blocking representation[17,18] further hinder reliable blocking prediction. Nonetheless, there have been efforts from the community to investigate possible sources of blocking predictability and to assess the performance of operational forecasts[12,13] that have accompanied continuous model improvements over the past few decades[19]. Recent studies showed appreciable prediction skills in subseasonal forecasts for blocking systems associated with extreme events[12,14] and in decadal forecasts of North Atlantic blocking[20].

[1] Atmospheric and Oceanic Sciences Program, Princeton University, Princeton, NJ, USA. [2]Geophysical Fluid Dynamics Laboratory, National Oceanic and Atmospheric Administration, Princeton, NJ, USA. [3]School of Earth and Environmental Sciences, Seoul National University, Seoul, South Korea. [4]School of Earth and Atmospheric Sciences, Georgia Institute of Technology, Atlanta, GA, USA. ✉e-mail: mp3238@princeton.edu

Representation and predictability of blocking in models on the seasonal time scale have received relatively less attention[21], particularly for the North Pacific (NP) blocking. The fact that seasonal prediction performance of NP blocking has not been explored much may not be surprising since blocking is an intrinsically intraseasonal phenomenon that is challenging to predict even on weather timescales. It is notable, however, that the seasonal statistics of temperature extreme events can be skillfully predicted in connection with low-frequency variability, like that of the El Niño-Southern Oscillation (ENSO), while the predictability of a single extreme event is limited to a few weeks[22,23]. In an analogous way, the statistics of atmospheric blocking may be also predictable on the seasonal time scale to some extent through the impact of slowly varying boundary conditions on the background mean state, upon which the blocking onset relies[21,24]. With this in mind, we focus on the seasonal prediction of blocking frequency during boreal winter, when atmospheric blocking occurs most frequently[2] and the magnitude of ENSO is strongest[25].

Although wintertime blocking in the North Atlantic (NA) region has received comparatively more attention than that in the North Pacific, NP blocking occurs with similar frequency and with significant impacts on the downstream North America region. A recent study using two different generations of Canadian Earth System Models (CanESM2 and CanESM5) showed that the observed linkage between NP blocking and North American cold spell frequency[9] is well reproduced by the models. This finding raises the possibility that a seasonal forecast modeling system may capture this linkage, depending on how well NP blocking frequency is simulated. In addition to the fact that a dominant physical process of blocking formation can differ across regions[2,26], the need for an investigation of seasonal prediction of NP blocking is further fueled by previous findings that the ENSO teleconnection plays an important role in modulating the NP blocking frequency[7,24,27] and that seasonal forecasting systems are capable of skillful forecasts of ENSO[28–30].

The present study examines the statistics and prediction skills of wintertime NP blocking frequency in seasonal hindcasts from the Seamless System for Prediction and Earth System Research (SPEAR)[31], a coupled global climate model developed by the Geophysical Fluid Dynamics Laboratory (GFDL) for seasonal to multidecadal prediction and projection. We used the medium-resolution version of SPEAR (SPEAR-MED but more simply referred to as SPEAR hereafter) due to current availability for both historical simulations and seasonal hindcasts, which has a 50-km atmospheric horizontal resolution and a 1.0° oceanic horizontal resolution with tropical refinement to 0.3°. Regarding the utility of the SPEAR forecast system, recent studies have demonstrated its ability to accurately simulate and provide skillful multiseasonal predictions for a variety of phenomena, including wintertime temperature extremes[23], atmospheric rivers[32], ENSO and its teleconnection patterns[29,33], and the Kuroshio extension variability[34], among others. These prior findings suggest that SPEAR may also be a valuable tool for exploring the seasonal predictability and prediction skill of atmospheric blocking. Therefore, this study leverages both observational data and SPEAR retrospective seasonal forecasts to evaluate forecast skill of NP blocking and to examine the sources of seasonal predictability. We also propose a hybrid dynamical-statistical model that leverages the skillful dynamical prediction of blocking precursors to yield skillful seasonal NP blocking predictions for lead times reaching 7 months.

Results

Blocking climatology and interannual variability in climate models

We first examine the climatology and interannual variability of wintertime blocking frequency in both reanalysis and climate models. For the detection of atmospheric blocking, three approaches based on the analysis of mid-tropospheric geopotential height have been commonly adopted in the community[2]: (1) the anomaly-based index, (2) the gradient-reversal index, and (3) the mixed (MIX) index. In order to reduce potential discrepancy and misdetection of blocking results by using a single approach, we identify blocking events in this study by the MIX index that considers both the magnitude of 500-hPa geopotential height (Z500) anomaly and the reversal of the meridional Z500 gradient around the local Z500 maximum[17,35] (see Methods). Figure 1A shows the ERA5 climatology of blocking frequency for boreal winter (December to February; DJF), which depicts the North Pacific and North Atlantic Oceans as the two preferred regions of blocking. Notably, the climatological blocking frequency in the NA sector is substantially larger than that of the NP sector, as indicated by a NA local maximum that is approximately 4.5 days larger than that of the NP. Such a regional difference is due to the adoption of the reversal gradient criteria in the MIX index[5,35] that preferentially excludes quasi-stationary high-pressure systems which frequently develop over the eastern Pacific[1,36]. The interannual variability of blocking frequency measured by its interannual standard deviation, on the other hand, reveals four distinct maxima: the NP, western Greenland, northern Europe, and Ural regions. Corresponding to the collocated regional maxima in geopotential height standard deviation[37], the identified regions show comparable magnitudes of standard deviation in blocking frequency, albeit with different climatological mean values.

In the second row, we show the 30-ensemble-member averaged climatology of blocking frequency and its interannual variability simulated by SPEAR (Fig. 1C, D). In general, both climatology and standard deviation of the blocking frequency are reasonably simulated in the midlatitudes. SPEAR well captures the two climatological peaks over the two ocean basins, as well as four regions of large interannual variability. These spatial features are similarly found in models from phase 6 of the Coupled Model Intercomparison Project (CMIP6)[38], as shown by the panels in the third row (Fig. 1E, F). If we use the root-mean-square error to evaluate the structural resemblance between observation and model, we see that the magnitudes of blocking biases in the SPEAR large ensemble are overall similar to those from CMIP6 multi-model mean. Given that models share typical structural blocking biases, the difference maps of climatology and interannual variability between ERA5 and SPEAR are displayed in Fig. 1G, H. In terms of climatological mean frequency, SPEAR overestimates NP blocking and underestimates NA blocking. These contrasting biases align with findings from a previous study using the earlier generation of climate models[2,17], as well as with results from recent studies using other GFDL comprehensive climate models that participated in CMIP6[39,40]. These studies revealed a connection of biases between blocking and zonally asymmetric background flow (i.e., stationary wave biases). In simulated interannual variability (Fig. 1H), negative biases are found over the four local maxima. The negative bias is particularly pronounced in Ural blocking, reflecting an influence from the model representation of the Ural Mountains[41]. This result indicates potential improvement of orographic impact through better-resolved orography in high-resolution models. Further discussion on the topic of model bias and potential improvements in blocking representation is presented below.

Despite sharing biases common to most state-of-the-art coupled climate models, SPEAR can simulate Northern Hemisphere blocking with statistics that are reasonably close to those of observations. We next explore the degree to which SPEAR can produce skillful seasonal predictions of NP blocking. To address this question, we employ the 15-member SPEAR hindcasts that cover the 1991-2021 period. These hindcasts are initialized with atmospheric restoring simulations and ocean data assimilation and then integrated for 12 months after initialization (Methods).

To investigate how SPEAR hindcasts simulate wintertime blocking frequency, the model blocking climatology in three different lead months is shown in the left column of Fig. 2. When identifying blocking from hindcasts, we additionally applied mean bias correction (Methods) which is known to improve model blocking biases in general[20,42]. Across the first three lead months, SPEAR hindcasts show a consistent spatial pattern of blocking climatology, generally sustaining regional features simulated by SPEAR historical simulations (Fig. 1C). However, the blocking frequency prediction skills measured by the anomaly correlation coefficient (ACC; Methods) decrease rapidly with increasing lead month, implying that the simulated interannual variability heavily depends on the initialization month (Fig. 2B, D, F). For instance, at the shortest lead (i.e., initialized on December 1st), the

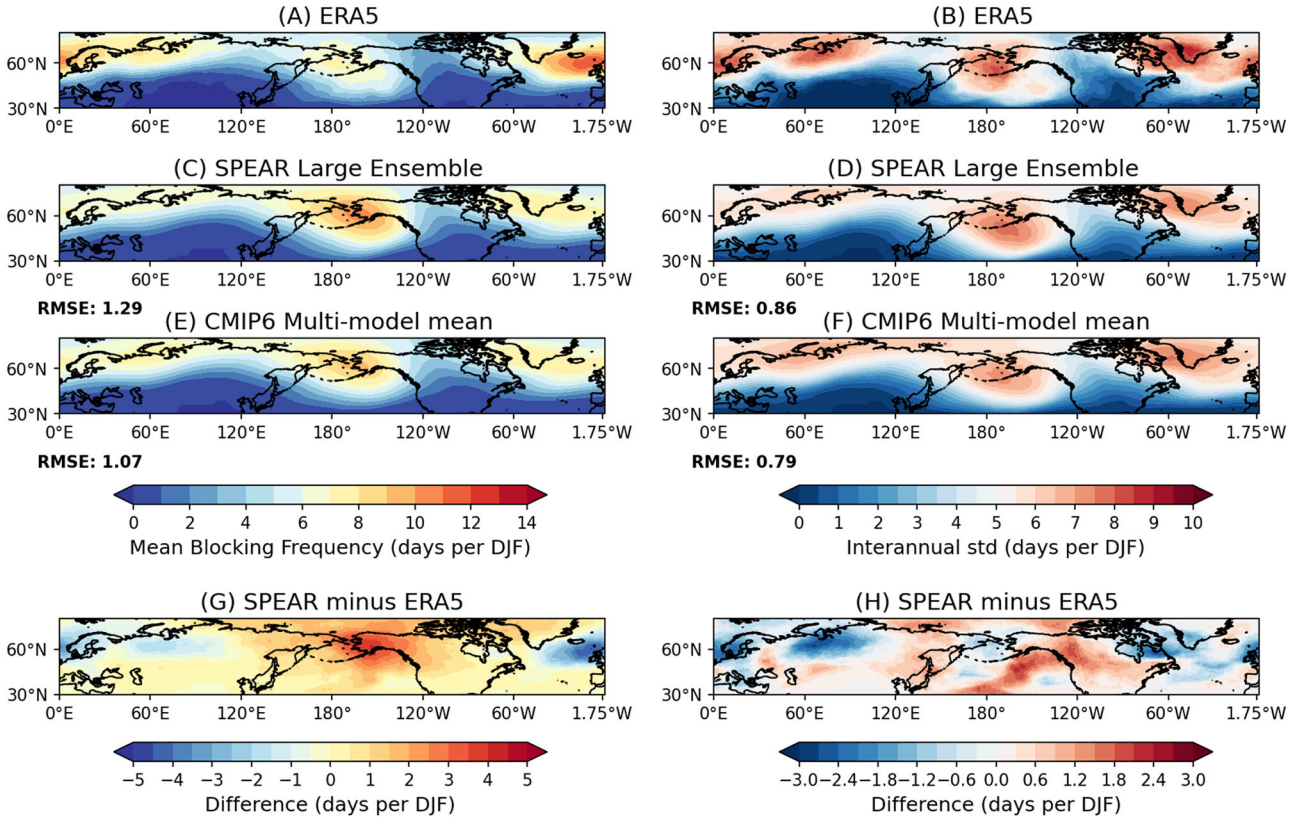

Fig. 1 | Statistics of wintertime (December-to-February; DJF) blocking from 1991/92-2020/21 in the ERA5 reanalysis and global climate models. DJF Climatology (left) and interannual variability estimated by the standard deviation (right) for (**A**, **B**) ERA5, (**C**, **D**) SPEAR large ensemble, (**E**, **F**) CMIP6 multi-model mean, and the differences (**G**, **H**) between SPEAR and ERA5. Regarding the interannual variability of the SPEAR large ensemble in (**D**), the standard deviation of blocking frequency has been computed for each ensemble member and then averaged over 30 ensemble members. In panels with calculations from climate models (**C**–**F**), the corresponding root-mean-square error over the Northern Hemisphere is shown at the bottom left.

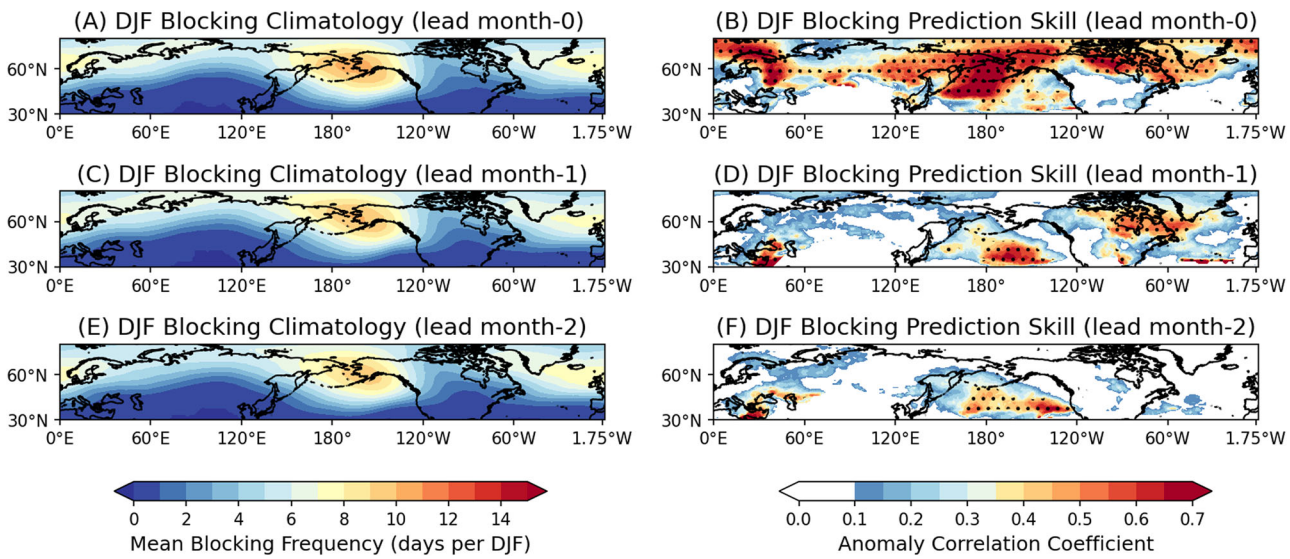

Fig. 2 | Climatology and Prediction skills of wintertime (DJF) blocking in SPEAR hindcasts (1991/92-2020/21). Wintertime blocking climatology of SPEAR hindcasts (1991/92-2020/21) after seasonal cycle bias correction (see Methods) for (**A**) lead 0 month (December 1st initialized), (**C**) lead 1 month (November 1st initialized), and (**E**) lead 2 months (October 1st initialized). The corresponding prediction skills measured by anomaly correlation coefficient are shown in (**B**), (**D**), and (**F**), respectively. Stippling indicates anomaly correlation coefficient statistically significant at the 5% level with an effective sample size as evaluated in Bretherton et al.[79].

hindcasts show significant prediction skills over the western NP, Canadian Arctic Archipelago, and northern Europe. In the lead 1 month (i.e., initialized on November 1st), only moderate prediction skills are found over the subtropical Pacific and northeastern North America. The lead 2 forecasts have even less area with positive ACC, mostly over the North Pacific Ocean with the northwest-southeast tilted structure. The rapid drop of the blocking prediction skill beyond lead 0 month likely indicates that most of the lead-0 skill is tied to the atmospheric rather than ocean or land initial conditions,

and the drop is associated with the absence of the accurate atmospheric background flow information at longer leads. By investigating the prediction skills of individual winter months at the shortest lead, we ascertained that most prediction skills in Fig. 2B originate from skills of December blocking frequency. The limited prediction skill of wintertime blocking frequency in high latitudes was similarly found in ref. 21 which used the seasonal prediction systems from the European Center for Medium-range Weather Forecasts (ECMWF).

Despite rapidly decreasing skills with lead time, we stress that SPEAR can skillfully predict blocking frequency at the shortest forecast lead over regions that have large observed interannual variability (Fig. 1B). It is also notable that the positive ACC in the North Pacific Ocean persists longer relative to other regions, suggestive of potential sources of blocking predictability therein. In the next subsection, we focus on the NP blocking frequency and discuss why its skillful prediction at lead 0 month can still be practical, owing to its downstream influence over North America.

Prediction skills and downstream impact of the western North Pacific blocking in SPEAR hindcasts

The western NP blocking, sometimes referred to as the Okhotsk or Kamchatka blocking in the literature, has been recognized as a driver of East Asian cold surges during boreal winter[4,5]. Figure 3A is a zoomed-in version of Fig. 2B, highlighting the lead-0 ACC in the NP domain. The area with the ACC larger than 0.7 is concentrated west of the Bering Sea, as denoted by the green box (40°–70°N/150°E–170°W). Calculations with the anomaly-based blocking index yield consistent results. We then explore whether the exceptionally high ACC in the western North Pacific is influenced by increasing greenhouse gas concentrations. To test this, the anomalous radiative component of Z500 derived from the SPEAR large ensemble is removed before blocking detection (Methods). As a result, model skills in the analyzed domain are overall maintained after removing the estimated contribution of global warming (Fig. 3B), again highlighting the substantial influence of initial conditions on the predictions of blocking frequency. To assess how model hindcasts simulate the year-to-year variability of western NP blocking, the time series of domain-averaged blocking frequency from both ERA5 and the SPEAR hindcasts are presented in Fig. 3C. The ensemble spread of blocking frequency in the SPEAR hindcasts initialized on December 1st includes the observed blocking frequency for most years, as illustrated by a boxplot at each year. Evaluated by the ensemble-averaged blocking frequency, the rank correlation skill of 0.59, statistically significant at the 0.1% level, supports the model's ability to predict the western NP blocking, in addition to supporting evidence from the high ACC. From an energetics perspective, this region is where the baroclinic growth and intensification of NP blocking preferentially occur[43].

The downstream impact of NP blocking is crucial for North American cold spells during boreal winter primarily through anomalous horizontal temperature advection[7–9]. Aiming to investigate the downstream influence of blocking, we conduct a composite analysis of western NP blocking events from the same hindcasts. The onset day of the blocking event (i.e., lag day 0) is defined as the first day when more than 60% of the area in the domain denoted by the green box is blocked. We note that the results are not qualitatively sensitive to the choice of the threshold to define the onset day. Figure 3D shows the observed composite of surface air temperature anomalies averaged over lag days 1 to 10 following blocking onset. Alaska and the Pacific Northwest experience significant cold anomalies in response to the cold advection driven by blocking. Farther downstream, the western United States also experiences significant warm anomalies due to the southeasterlies associated with the trough over central Canada. This dipole temperature anomaly pattern in observations is well reproduced by the SPEAR hindcasts (Fig. 3E). The intensity and centers of circulation anomalies associated with NP blocking are also captured well. Insomuch as the hindcasts accurately simulate seasonal blocking frequency, its downstream impact is likely to be well reflected in the hindcasts, contributing to a further improvement in the seasonal prediction of North American cold extremes[23].

Additionally, the lagged composites of precipitation anomalies show that the western United States and Southwest Canada experience significantly increased precipitation anomalies in response to the moisture advection by blocking-related circulations, whereas the central North Pacific Ocean close to the blocking center experiences significantly reduced precipitation anomalies (Fig. 3F). These observed spatial features are again well reproduced by the SPEAR hindcasts (Fig. 3G), which further increases confidence in the model performance of simulating the downstream influence of North Pacific blocking.

Atmospheric sources of predictability for the western North Pacific blocking

The above results of the western NP blocking are based on the hindcasts at lead 0 month (i.e., December 1st initialization), which relies on the atmospheric initial conditions to produce skillful predictions of the western NP blocking. To shed light on what features of the atmospheric initial conditions are most critical for the skillful prediction of blocking, we examine the representation of the NP storm track (i.e., 850-hPa high-frequency eddy heat flux obtained by 10-day high-pass filtered meridional wind and temperature) in hindcasts, given the importance of synoptic-scale eddy feedback on the downstream formation of blocking[26,44–46]. For the composite analysis, the 7 winters with the highest and lowest blocking frequency are selected from observations to highlight the spatial difference of storm track eddies, and the period of December 1-5 is chosen as representative of the initial conditions.

The lead 0 hindcasts clearly show that compared to low-blocking winters, lower tropospheric eddy heat fluxes are developed more vigorously and reach farther poleward during high blocking winters (Fig. 4A, D, G). In the 150°E–170°W averaged values, we find that the local maximum of 850-hPa eddy heat flux in high-blocking winters is stronger by 1 K m s^{-1} and shifted poleward by approximately 6°, relative to that in low-blocking winters (Fig. 4I), along with distinct differences in magnitudes poleward of 50°. In contrast, such spatial differences in the early December storm tracks are rarely seen from the composites of hindcasts averaged over leads of 1-3 months (Fig. 4B, E, H), which likely explains why the skill drops rapidly with lead time. The longitudinally averaged values in leads 1–3 are also similar to the climatology (Fig. 4J), and this muted difference is similarly found if individual lead months are used for the analysis. Similarly, the location and intensity of the low-level jet from 850-hPa zonal wind show stark differences between high- and low-blocking winters (Fig. S1). During high-blocking winters, the zonal wind within the western NP domain slows down considerably, indicating favorable conditions for blocking development[1]. On the other hand, this distinct difference in zonal wind between low- and high-blocking winters from lead 0 is not found in leads 1-3. Therefore, the atmospheric background flow in the initial conditions strongly modulates the model ability of seasonal prediction of blocking, as noted by earlier studies of the subseasonal forecasts[15,47].

Given the apparent strong dependence of seasonal prediction skill on the atmospheric initial conditions, one may hypothesize that the seasonal predictability of North Pacific blocking is intrinsically limited by the short memory of chaotic atmospheric variability. Alternatively, if the sharp drop in skill is more of a reflection of model errors inhibiting the simulation of all the dynamical processes that result in blocking, and if the model is more skillful at simulating the large-scale precursors of blocking, then there may still be opportunities to produce skillful seasonal predictions of NP blocking at longer lead times. For example, seasonal prediction models, including SPEAR, have shown good performance in predicting tropical sea surface temperature (SST) variability such as ENSO[28–30], and the ENSO teleconnection can modulate the frequency of NP blocking[7,24,27]. In the following subsection, we explore if the ENSO-blocking linkage can be utilized as a prediction source of the western NP blocking.

The ENSO-blocking relationship in observation and SPEAR

A distinct characteristic of the boreal winter ENSO teleconnection pattern is the northwest-southeast tilted anomalous atmospheric pressure pattern

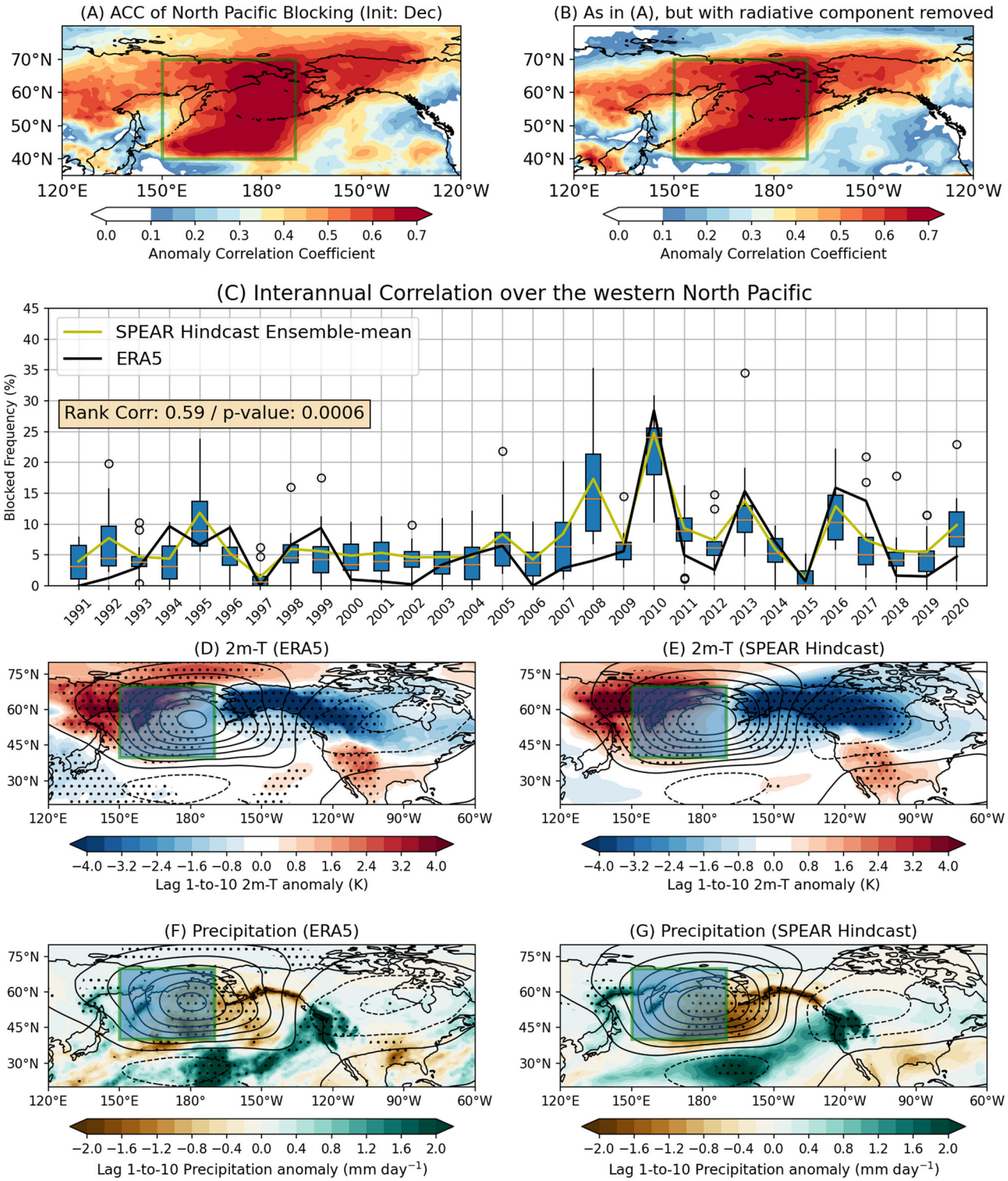

Fig. 3 | Prediction skills and the downstream impact of the western North Pacific blocking. A ACC of DJF North Pacific blocking from lead 0 month. **B** As in (**A**), but after removing global warming contribution by using the SPEAR large ensemble. The green box denotes the domain of the western North Pacific. **C** DJF time series of the domain-averaged western North Pacific blocking frequency for ERA5 (black line) and SPEAR hindcast ensemble-mean from lead 0 month (yellow line). The model ensemble spread for each winter is denoted by a boxplot, while white circle indicates a model outlier. The rank correlation with its *p*-value is shown in the upper left corner. **D** 10-day lagged composite of ERA5 surface air temperature anomalies after the development of the western North Pacific blocking events ($n = 24$). Black contours denote Z500 anomalies composited for lag days −2 to +2 with an interval of 40 m. Stippling indicates the statistical significance at the 5% level evaluated by a Monte Carlo test with 5,000 random subsamples of the same sample size. **E** As in (**D**), but for the ensemble-mean of SPEAR hindcasts, while composite analysis and Monte Carlo significance tests have been performed for each ensemble member. **F**, **G** As in (**D**) and (**E**) but for 10-day lagged composites of ERA5 and SPEAR hindcast precipitation anomalies, respectively.

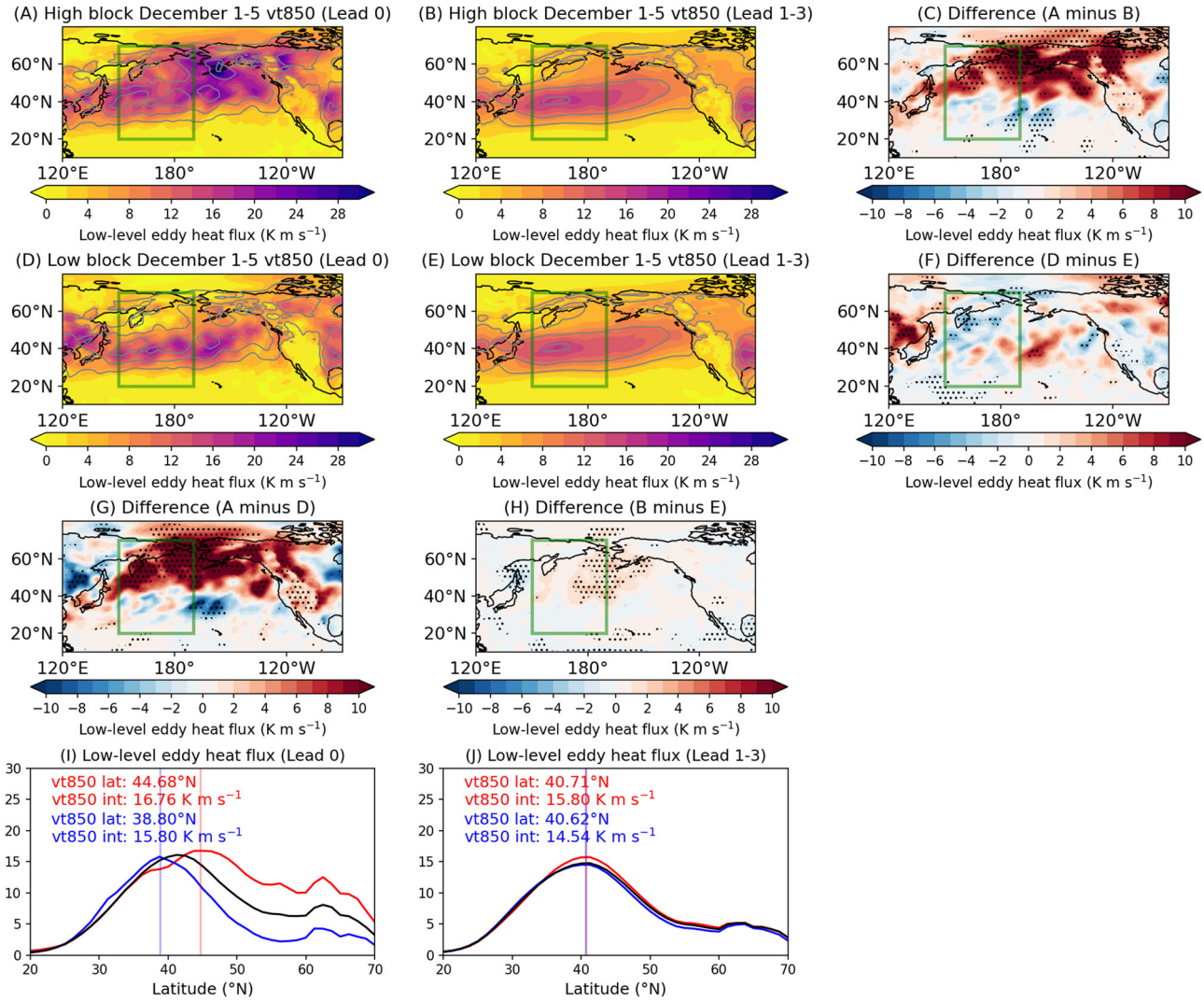

Fig. 4 | Model representation of synoptic-scale eddies dependent on lead time. **A**, **B** Composites of December 1st–5th 850-hPa high-frequency eddy heat flux ($v_H^* T_H^*$; where subscript H stands for 10-day the high-pass filtered variable and the asterisk stands for the deviation from the zonal mean) from SPEAR hindcasts of (**A**) lead month 0 (December 1st initialized), and (**B**) lead months 1–3 average (November 1st, October 1st, and September 1st initializations) for the top 7 winters of western North Pacific blocking frequency in the ERA5 reanalysis. **C** Difference between (**A**) and (**B**). Gray contours indicate the climatological December 1st–5th eddy heat flux with an interval of 5 K m s^{-1}. The results are qualitatively consistent if a single lead month is used for (**B**). **D**–**F** As in (**A**–**C**), but for the bottom 7 winters of western North Pacific blocking winters in the ERA5 reanalysis. **G**, **H** Differences between the top and bottom 7 winters. Note that the top and bottom ranked winters are chosen from the observed blocking frequency to emphasize the importance of synoptic-scale eddy representation. **I**, **J** Longitudinally averaged 850-hPa high-frequency eddy heat flux over the western North Pacific domain (green boxes; 20°–70°N, 150°E–170°W) for (**I**) lead month 0 and (**J**) lead months 1–3 average. Red text indicates the latitude and magnitude of the peak values for the top 7 winters, while blue text indicates the same for the bottom 7 winters. Stippling indicates the statistical significance at the 5% level evaluated by a two-sided Welch's *t*-test.

over the NP, which is well reproduced by the SPEAR model[31,33]. To investigate whether this ENSO teleconnection leads to a significant relationship between ENSO and NP blocking, we first analyze the rank correlation between the 3-month running mean Niño-3.4 index, or Oceanic Niño Index (ONI), and blocking frequency from observations (Fig. 5A). The result reveals that significant negative correlations are mostly found over the Russian Far East and North Pacific Ocean, indicating that suppressed blocking frequency tends to be favored in the boreal winters of El Niño. In Fig. 5B, we replace the observed ONI with the ensemble-mean lead 0-month SPEAR hindcast ONI (i.e., initialized on December 1st), considering that SPEAR maintains a prediction skill of the wintertime ONI variability exceeding 0.7 until lead month 7 (i.e., May 1st initialization; Fig. S2). As expected from high prediction skill of ENSO at the shortest lead time (e.g., ref. 29; Fig. S2), the pattern of significant correlations with the SPEAR ONI is nearly identical to that with the observed ONI, albeit with a weaker correlation for high-latitude blocking poleward of 65°N. Figure 5C depicts how this ENSO-blocking linkage is represented in the hindcasts on average. The simulated linkage tends to be shifted westward compared to the observation, particularly over the central NP and northern Canada, which is partly associated with the westward-shifted biases in the maximum ENSO teleconnection over the Pacific-North American region[31,33]. This figure also shows that the linkage between ENSO and the eastern Pacific blocking is muted in the SPEAR hindcasts. This model error in the ENSO-blocking linkage would be one of the reasons for the limited prediction skill of NP blocking frequency.

Given that ENSO has a strong connection to NP blocking and that SPEAR skillfully predicts ENSO for lead times reaching 9 months (see Fig. S2), we may expect that SPEAR also can skillfully predict NP blocking for longer lead times than indicated in Fig. 2. However, as partly shown in the differences of the atmospheric background flow depending on lead

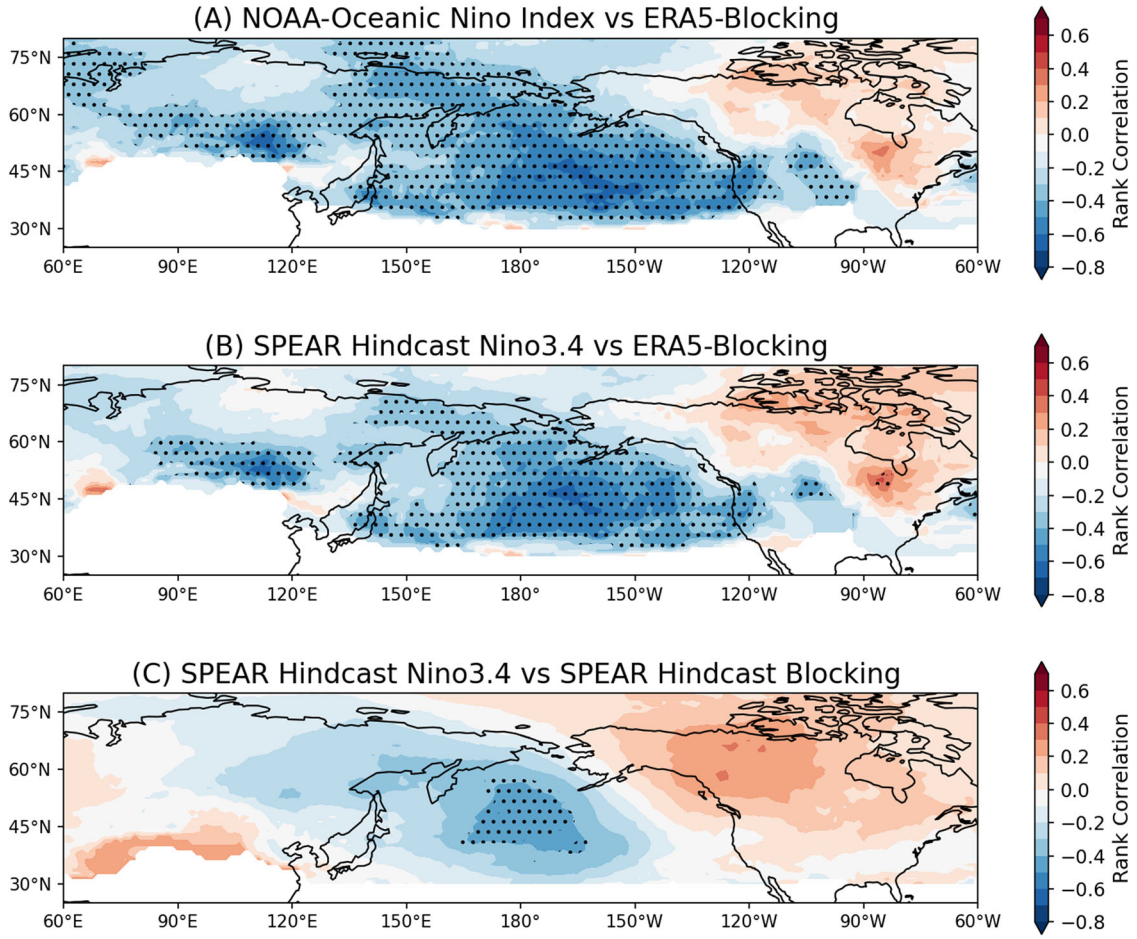

Fig. 5 | Relationship between ENSO and North Pacific blocking frequency during boreal winter. A A map of rank correlation between the NOAA DJF Oceanic Niño Index and ERA5 blocking frequency. **B** A map of rank correlation between the 15-ensemble-member averaged DJF Oceanic Niño Index from SPEAR hindcasts initialized on December 1st and blocking frequency in the ERA5 reanalysis. **C** A map of the 15-ensemble-member averaged rank correlation between the DJF Oceanic Niño Index from SPEAR hindcasts of the December 1st initialization and DJF blocking frequency in the SPEAR hindcasts from the same initialization month. Stippling indicates rank correlations that are statistically significant at the 10% level with an effective sample size as evaluated in Bretherton et al.[79] .

months (e.g., Fig. S1), model errors in the atmospheric mean state quickly grow due to an inherent model drift. Figure 6A shows the root-mean square deviation of the 850-hPa zonal wind field in the Northern Hemisphere with respect to the same field from the historical simulation, specifically on the seasonal cycle of December 1st-January 29th (i.e., 60 days). We see that after about one month from initialization, the characteristics of zonal winds simulated in the SPEAR hindcasts show very similar differences regardless of lead time, reflecting the model drift toward the uninitialized SPEAR climatology. Such behavior is systematically found in other regional metrics such as the Pacific low-level jet location (Fig. 6B), intensity, and atmospheric circulation fields (e.g., an upper-level zonal wind). Since the model drift of the atmospheric mean state becomes pronounced with lead time, we hypothesize that the model fidelity in representing the relationship between ENSO and synoptic-scale eddy heat flux on the seasonal time scale also may deteriorate rapidly with lead time in response to this model drift.

We test this hypothesis by regressing the SPEAR wintertime 850-hPa eddy heat flux against the ONI at different lead months (Fig. 7). We find that lower tropospheric fluxes at the entrance and northeastward flank of the North Pacific storm track are significantly modulated by ENSO at lead 0 (Fig. 7B), generally in accordance with the observed linkage of synoptic-eddy heat fluxes to ENSO (Fig. 7A). This result indicates that the SPEAR hindcasts at lead 0 partly capture poleward eddy heat fluxes associated with ENSO, which dominantly occur over the Gulf of Alaska and serve as energy source for wintertime blocking through baroclinic energy conversion[43]. However, even at a lead of just 1 month earlier, the ENSO/850-hPa eddy heat flux linkage overall is displaced equatorward, as depicted by weakened regressions poleward of 30°N and intensified regressions west of the dateline (Fig. 7C). This equatorward drift from the regressions continues at longer lead months and becomes more pronounced (Fig. 7D), indicating that a growing error in the ENSO-eddy heat flux linkage (Fig. 7E) is likely to induce errors in the ENSO-blocking linkage and a reduced NP blocking forecast skill. Furthermore, a direct impact of model drift to the ENSO-eddy heat flux linkage is depicted by the root-mean square deviation (RMSD) of the regressions between the ONI and eddy heat flux for different lead months (Fig. 6C, D). The regressions in lead month 0 only substantially deviate from those of the SPEAR historical simulation up to day 20 (i.e., December 20th), while other lead months show nearly constant RMSD values, indicating that in spite of high ENSO prediction skills by SPEAR (Fig. S2), the model drift in the atmospheric mean state directly disrupts the linkage between ENSO and synoptic-scale eddy activity.

Multiseasonal forecasts of North Pacific blocking using a hybrid dynamical-statistical model

The strong ENSO seasonal prediction skill from the current dynamical prediction systems[28–30] and the significant relationship between ENSO and NP blocking demonstrated above motivate us to test a hybrid dynamical-statistical prediction approach. A hybrid dynamical-statistical model combines output from dynamical forecasts and statistical relationships between predictors and predictand (e.g., ref. 48). In this study, we predict wintertime blocking frequency by using a linear regression model that has two

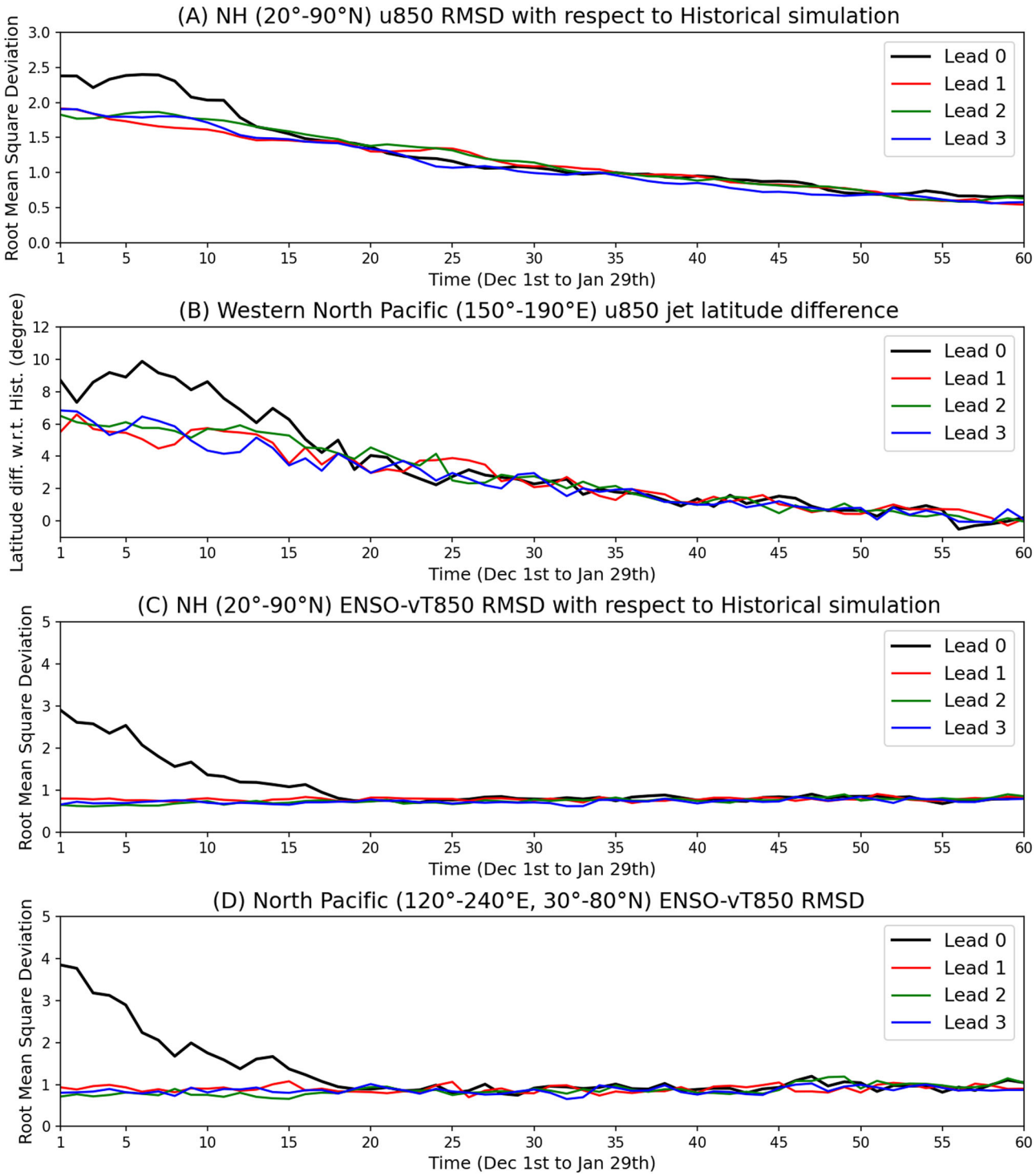

Fig. 6 | Model drift of the background flow and its influence on the linkage between ENSO and high-frequency eddy heat flux in SPEAR hindcasts. A Temporal evolution of the root-mean square deviation (RMSD) of the 850-hPa Northern Hemisphere (20°–90°N) zonal wind. The RMSD values have been computed from December 1st to January 29th for the hindcasts with different lead months, relative to the corresponding DJF-mean flow in the SPEAR historical simulation (Unit: m s^{-1}). **B** Temporal evolution of differences in the western North Pacific (150°E–170°W) low-level jet latitude from December 1st to January 29th for the hindcasts at different lead months. Note that the DJF climatological low-level jet latitude in the SPEAR historical simulation has been used to compute its difference from that in the hindcasts. **C** Temporal evolution of the RMSD of the regression coefficients of the 850-hPa high-frequency eddy heat flux ($v_H^* T_H^*$) on the SPEAR Oceanic Niño Index over the Northern Hemisphere (20°–90°N). The RMSD values have been computed from December 1st to January 29th for the hindcasts at different lead months, relative to the regression coefficients in the SPEAR historical simulation at the corresponding day (Unit: K m s^{-1} per K). **D** As in (**C**), but for the North Pacific domain (120°E–120°W, 30°–80°N).

predictors associated with NP blocking frequency—the ONI and western NP precipitation. While the ONI plays a major role as a predictor in this hybrid model (e.g., Fig. S3), we found it is also advantageous to consider local latent heating that serves as a wave source and contributes to the amplification of downstream blocking systems, as supported by both observations and a theoretical framework[49,50].

The role of latent heating in atmospheric blocking suggested by the previous studies operates mostly on the shorter intraseasonal time scale.

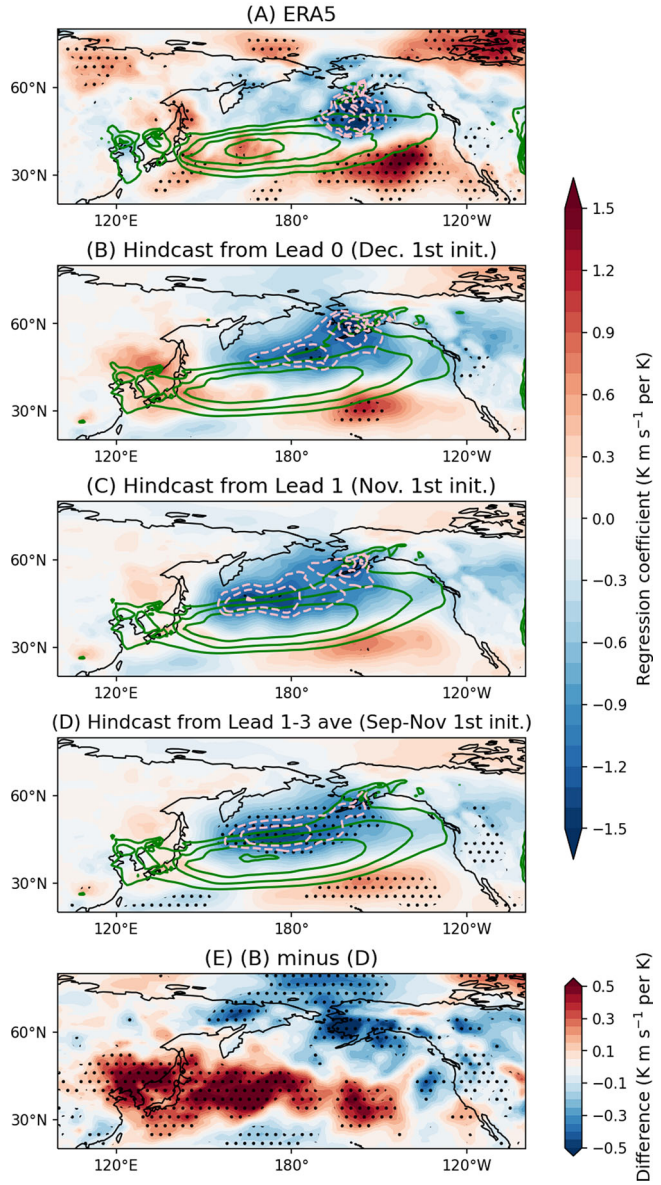

Fig. 7 | Model representation of the ENSO-lower tropospheric eddy heat flux relationship. A A regression map of the ERA5 DJF-mean 850-hPa high-frequency eddy heat flux ($v_H^* T_H^*$) onto the NOAA DJF Oceanic Niño Index. Prior to regression, each time series is linearly detrended. Green contours indicate climatological eddy heat flux larger than 8 K m s^{-1} with an interval of 2 K m s^{-1}, and pink contours indicate regression coefficients larger than 1 K m s^{-1} per K with an interval of 0.2 K m s^{-1} per K. Stippling indicates the statistical significance at the 10% level evaluated by a two-sided Student's *t* test. In this regression analysis, the 29-year period (i.e., 1992/93-2020/21 DJF) is used due to the data loss at the beginning of the time series arisen from a Lanczos band-pass filter. **B** A regression map of the SPEAR 15-ensemble-member averaged DJF-mean 850-hPa high-frequency eddy heat flux onto the corresponding DJF ONI from the December 1st initialization. **C**, **D** As in (B), but from (C) November 1st initialization and (D) the average of September 1st-November 1st initializations. **E** Difference in regression coefficients between (B) and (D).

Nevertheless, a significant linkage between NP blocking and its upstream precipitation (Fig. S4) encourages us to test its usefulness as a local thermodynamic predictor for the interannual variability of atmospheric blocking. This choice has been further prompted by a recent finding that there is a significant interannual relationship between NP blocking and its upstream boundary condition over the Okhotsk Sea region (e.g., ref. 51). The statistical significance of upstream precipitation as a second predictor of NP blocking has been confirmed by an F-test (see Methods). While SPEAR exhibits good Niño 3.4 index prediction skill up to lead month 9 (Fig. S2), reasonably high and significant prediction skill of the seasonal-mean western NP precipitation, independent from ENSO, is also found up to lead month 3 (Fig. S5). This persistence of ENSO-independent Okhotsk Sea precipitation prediction skill is due to its connection with slowly varying North Pacific sea surface temperature variability (Fig. S6), which can be skillfully predicted by SPEAR (Fig. S7). Although there might be other significant predictors of NP blocking worth exploring in future studies, we focus on these two predictors for the hybrid model in this study because of the strong theoretical grounds for their inclusion and the support from previous studies[2,17,24,27,49,50,52]. We make predictions of DJF blocking frequency for leads of up to 9 months (1 March initialization) using the predictors from each initialization. Moreover, to avoid overfitting, we generate cross-validated forecasts by using a leave-one-year-out approach in which the model is trained with data that excludes the prediction year (Methods).

Figure 8 shows the rank correlation skill of blocking frequency for leads of 0-9 months from our hybrid dynamical-statistical model in the left column and that from the dynamical model in the right column. It is clearly seen that the hybrid model prediction sustains significant correlation skill over the Russian Far East and North Pacific Ocean for leads of up to 3 months (i.e., September 1st initialization; Fig. 8A–F), accompanying the prominent northwest-southeast tilt reminiscent of wintertime ENSO teleconnection. Although the performance of the dynamical model output is superior to the hybrid model at a 0-month lead (i.e., December 1st initialization; Fig. 8B), especially for high-latitude blocking, its prediction skill rapidly deteriorates beyond lead 0 month, consistent with the previous model assessment by the ACC (Fig. 2). For instance, at leads of 1 and 3 months, most significant correlation skills derived directly from SPEAR are found equatorward of 60°N and west of the dateline (Fig. 8D, F) but not farther north and east, reflecting the displaced relationship between ENSO and synoptic-scale eddy heat flux (Fig. 7). Even at leads of 6 and 9 months, the hybrid model shows regions of persistently positive skills over the North Pacific Ocean (Fig. 8G–J), and this long-lasting correlation raises the possibility of operational multiseasonal forecasts of NP blocking and its downstream impacts.

We also compare the domain-averaged blocking frequency between the dynamical and hybrid model forecasts. The high-latitude NP blocking near the Bering Sea (i.e., 50°–75°N/150°E–150°W) is chosen because of its local climatological peak during boreal winter. Figure 9A shows the standardized and linearly detrended time series of the high-latitude NP blocking frequency from both the hybrid and dynamical models at leads of 0, 1, and 3 months. As captured by the temporal correlation coefficients for each time series, the ensemble-mean SPEAR hindcast at lead 0 (black solid line) shows the largest correlation, 0.68. This high skill is followed by a marked decrease in dynamical forecast model performance with lead time, as seen from previous results. The hybrid model prediction performance, on the other hand, is relatively well maintained across leads, suggesting that the NP blocking may be skillfully predicted by the hybrid model up to 7 months in advance (Fig. 9B). We found that the dynamical forecast model occasionally shows negative correlation skills in longer lead months, unlike the hybrid model, which consistently retains positive skills (Table S1). The result is qualitatively insensitive to the choice of the latitudinal domain (e.g., 40°-80°N). The persistence of prediction skill in the hybrid model is inherently derived from the dynamical model's ability to predict the interannual variability of tropical SST, including ENSO, and, to a lesser extent, the North Pacific SST. The importance of ENSO prediction is also evidenced by the timing when the hybrid model's prediction skill notably diminishes at lead 8 month (i.e., initialized on April 1st), which corresponds to a steeper decline of the Niño 3.4 index prediction skill by SPEAR at the same time (Fig. S2B). This decline is associated with the challenge that many seasonal prediction systems in predicting ENSO during spring initializations, often referred to as the "spring predictability barrier"[25,29]. Another notable aspect of the hybrid model performance is that its correlation skill shows a temporal peak at a

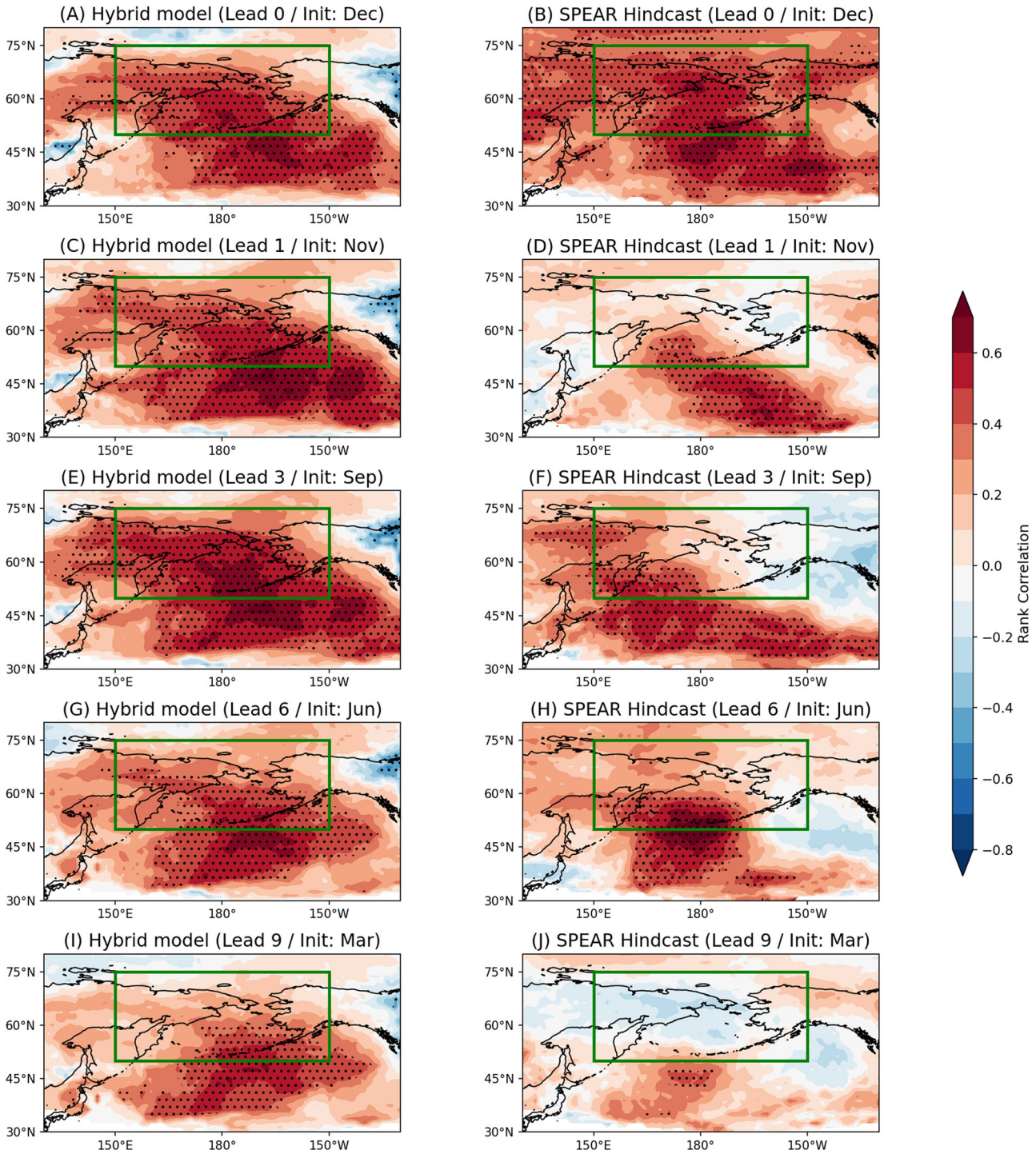

Fig. 8 | Comparison of rank correlation skills between the hybrid statistical-dynamical model hindcasts and SPEAR dynamical hindcasts for different lead times. Rank correlation maps of DJF blocking frequency (**A**) between ERA5 and the hybrid model using the forecasted Niño 3.4 index and upstream precipitation from the December 1st initialization, and (**B**) between the ERA5 reanalysis and SPEAR hindcasts of the December 1st initialization. For the hybrid model, the linear dependence between the two predictors has been removed by the linear regression method. The green boxes denote the domain of high-latitude North Pacific blocking frequency used in Fig. 9. **C**, **D** As in (**A**, **B**) but for a 1-month lead (November 1st initialization), (**E**, **F**) 3-month lead (September 1st initialization), (**G**, **H**) 6-month lead (June 1st initialization), and (**I**, **J**) 9-month lead (March 1st initialization). Stippling indicates a rank correlation statistically significant at the 5% level with an effective sample size as evaluated in Bretherton et al.[79].

lead of 3 months (i.e., initialized on September 1st), as hinted by the rank correlation map (Fig. 8E). This peak is primarily driven by precipitation over the Okhotsk Sea, serving as an additional predictability source of NP blocking variability on the interannual time scale. In agreement with the decrease of the hybrid model prediction skill at a 4-month lead, the prediction skill of SPEAR for this upstream precipitation persists for 3 months (Fig. S5). At the 4-month lead time (i.e., initialized on August 1st), the rank correlation skill of this upstream precipitation against the observation drops to 0.21, in contrast to the correlation value 0.47 ($p < 0.01$) at the 3-month lead time.

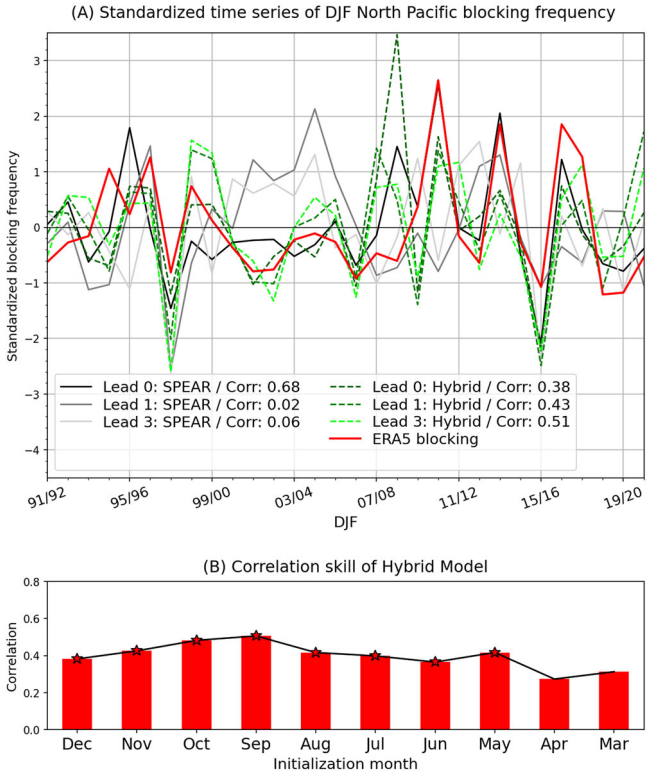

Fig. 9 | Simulated interannual variability of high-latitude North Pacific blocking from the hybrid statistical-dynamical model and SPEAR dynamical hindcasts for different lead times. A Standardized time series of DJF North Pacific domain-averaged (i.e., 50°–75°N/150°E–150°W indicated by the green box in Fig. 8) blocking frequency for the ERA5 reanalysis (red line), SPEAR hindcasts (solid contours), and the hybrid model hindcasts (dashed contours) for different lead months. Each time series is also linearly detrended, and temporal correlations between hindcasts and reanalysis are shown in the legend. **B** Correlation of DJF North Pacific blocking frequency between the ERA5 reanalysis and the hybrid dynamical-statistical model for leads ranging from 0 (Dec initialization) to 9 (Mar initialization) months. A star symbol indicates that the Pearson correlation is statistically significant at the 5% level.

Discussion

This study explores the prediction skill of wintertime North Pacific (NP) blocking frequency in the GFDL SPEAR seasonal forecast system. While there have been a number of studies exploring the short-to-medium-range forecasts of atmospheric blocking events due to their potential to provide early warnings of high-impact extreme weather events closely linked to blocking (e.g., refs. 12–15,53), our study attempts to expand this effort to the seasonal time scale of blocking frequency. The blocking detection algorithm considers both the reversal criteria of the geopotential height gradient and amplitude of geopotential height anomaly to identify blocking events. We have shown that the skill at a 0-month lead (i.e., initialized on December 1st) is pronounced over the western NP region on the poleward flank of the Pacific storm track, but this skill drops rapidly with increasing lead time. This result motivated us to explore whether the drop in skill may reflect an intrinsic limitation of the seasonal predictability of NP blocking or, alternatively, the high initial skill may indicate the potential for skillful multi-seasonal forecasts of NP blocking if we can overcome key model biases. Given the strong connection between NP blocking and slowly varying sea surface temperatures, particularly from ENSO, we hypothesized that model drift in the background state was likely a major inhibitor of seasonal blocking skill. We then demonstrated that the interaction of these growing errors in background state with slowly evolving ENSO signal induces errors in the linkage between ENSO and synoptic-scale eddy heat fluxes that are critical for NP blocking frequency anomalies. Therefore, the accurate simulation of the background mean state, the slowly evolving tropical SST anomalies, and the interaction between these SST anomalies and the storm track synoptic eddies are essential for maintaining skillful predictions of NP blocking beyond the shortest lead times.

In spite of limited deterministic skills in blocking frequency prediction due to the apparent model deficiencies in simulating high-frequency eddy heat fluxes, we still achieve skillful multiseasonal forecasts of NP blocking frequency through a hybrid dynamical-statistical prediction approach. This adaptation capitalizes on the significant interannual linkage between ENSO and upstream precipitation with blocking, as well as the ability of the model to predict these blocking precursors at long leads more skillfully than the blocking frequency itself. The hybrid model is constructed as a multiple linear regression model that has the predictors – Oceanic Niño Index and upstream precipitation – incorporated from the dynamical model (i.e., SPEAR hindcasts with leads extending to 9 months). Regarding the prediction of high-latitude NP blocking frequency, the hybrid model forecasts outperform the dynamical model forecasts for leads from 1 to 9 months and are inferior to the dynamical model forecasts only at lead 0 when the midlatitude background flow from initial conditions plays a crucial role as a dominant source of predictability. The promising skills of the hybrid dynamical-statistical model suggest some potential operational application that overcomes the limited blocking prediction skill in the dynamical modeling systems on seasonal time scales.

With the above in mind, we discuss some limitations of the hybrid model. First, as expected from its design, the hybrid model does not include predictors that represent the atmospheric dynamic contribution to the formation and maintenance of blocking, including interactions among eddies on different time scales, due to its short-term predictability in the dynamical model[47,54]. Second, similar to the aforementioned caveat, a multiple linear regression method of the model inherently does not consider nonlinearity of blocking, including its nonlinear linkages to the thermodynamic predictors. Third, there still might be other predictors influencing NP blocking frequency. For example, the recent decline in Arctic sea ice concentration affects the extratropical circulation on a regional scale, which changes zonal winds adjacent to the area of sea ice loss and thus modulates blocking frequency (e.g., refs. 55–57). The proposed mechanism involves a more vigorous excitation of upward propagating planetary-scale waves, which often results in a deceleration of the stratospheric polar vortex and the following downward influence on regional blocking. If this mechanism operates in the seasonal prediction model, the variability of regional sea ice may also serve as an influential predictor of NP blocking. However, the current version of the atmospheric model in SPEAR does not resolve stratospheric-tropospheric coupling well enough to take the mechanism into consideration. A version with a finer stratospheric resolution that may be able to capture this proposed linkage is under development, and we leave this investigation for future studies. Fourth, due to the limited time period available for the hindcasts (i.e., 30 years), more detailed linkages between NP blocking and El Niño diversity (e.g., Central Pacific El Niño versus Eastern Pacific El Niño; ref. 24) have not been considered. Lastly, with the limited data available, it is challenging to avoid the overfitting problem caused by overlapping training and testing periods[58]. Therefore, a prolonged period of hindcast data availability will be merited.

Despite these limitations, our finding that the SPEAR hindcasts are able to reproduce the observed downstream impact of NP blocking suggests that an enhancement of the blocking prediction skill would entail an improved skill in the seasonal prediction of North American climate, including precipitation and temperature variability. A previous study investigated the prediction skill of North American temperature during ENSO winters by using 6 different models in the North American Multi-Model Ensemble (NMME) project[59] and found that their performance at a 1-month lead is particularly poor for predicting temperature patterns during La Niña winters[60] when the occurrence of NP blocking is preferential. We speculate that this deficiency may have resulted, in part, from the overall underrepresented variability of NP blocking frequency in the hindcasts and from potential biases in the ENSO-blocking relationship

(e.g., Fig. 5C) due to the westward shifted ENSO teleconnection in climate models[61]. This may provide an opportunity to explore the linkage of prediction skills between North American temperature and NP blocking across the NMME models. In addition, although not explored in this study, incorporating the duration of NP blocking into the hybrid model approach may improve the prediction skills of North American temperature variability, since the quasi-stationarity of blocking has often been linked to the occurrence of temperature extremes[6,12–14,17]. Given that the mean westerly flow and vertical wind shear are closely linked to the persistence of regional atmospheric blocking and related temperature extremes through meridional surface temperature gradients[6], a similar hybrid model approach incorporating local boundary conditions as predictors has potential to address the predictability of the seasonal-mean blocking duration.

A more general approach to improve the prediction skill of blocking may be a reduction of climatological biases in the modeling systems (Fig. 1), which is closely related to atmospheric circulation mean state biases to leading order[39,62]. In the case of another GFDL model closely related to SPEAR, for instance, Narinesingh et al.[40] examined the zonal-mean removed 500-hPa geopotential height climatology in GFDL-CM4 as a model representation of stationary waves (i.e., zonal asymmetry in the climatological mean state) and found positive biases for the NP stationary waves and negative biases for the NA sector. Their result indicates a close relationship between blocking biases and stationary wave biases, supported by the finding that stationary waves affect the diffluence of the jet stream, upon which the magnitude of the zonal local wave activity flux hinges (e.g., ref. 1). Together with the importance of atmospheric mean state bias, we recognize that there has been a myriad of other model shortcomings discussed in the literature[2], including but not limited to climatological SST biases[63–65], limited atmospheric and oceanic resolutions[21,41], errors in parameterized orographic drag[66], and underrepresentation of diabatic processes[67,68]. For a systematic assessment of model performance, a comprehensive testbed is essential to investigate the extent of improvement in blocking representation achievable through testing various model configurations (e.g., ref. 21). In this context, our future study will examine blocking representation in alternative versions of the GFDL SPEAR model. This will include simulations aimed at significantly reducing climatological SST biases using the flux adjustment technique (e.g., ref. 69) and simulations implementing higher atmospheric and oceanic resolution, which are currently under development.

Methods

Observational data

In this study, we use the fifth generation of the European Centre for Medium Range Weather Forecasts (ECMWF) Reanalysis (ERA5)[70] for observational reference. Daily mean surface temperature, horizontal winds, mean sea level pressure, and geopotential height data are obtained by averaging four 6-hourly time steps, while daily accumulated precipitation data is obtained by integrating outputs from hourly time steps. The analyzed period of boreal winter (December-January-February; DJF) ranges from December 1991 to February 2021 (total 30 DJFs), and the horizontal resolution of the analyzed variables is 1.25° × 1.25°. For ENSO analysis, the Oceanic Niño Index provided by the National Oceanic and Atmospheric Administration Climate Prediction Center (NOAA-CPC) is used, which is computed as the 3-month running mean of ERSSTv5 SST anomalies in the Niño 3.4 domain (5°N-5°S, 120°-170°W).

The SPEAR model

A suite of large ensemble simulations from the Seamless System for Prediction and Earth System Research (SPEAR)[31] model is employed throughout the study. The SPEAR modeling system has been recently developed by the GFDL with the aim to investigate seasonal to multidecadal predictability and variability of various climate phenomena, providing both historical simulations and seasonal hindcasts that are primarily forced by external radiative forcing and initial boundary conditions, respectively. It consists of the GFDL state-of-the-art component models such as atmospheric (AM4), land (LM4), sea ice (SIS2), and oceanic (MOM6) component models. This study used the medium-resolution version of SPEAR (SPEAR-MED) characterized by a 50-km atmospheric horizontal resolution and a 1.0° oceanic horizontal resolution with tropical refinement to 0.3°. SPEAR-MED has participated in the North American Multi-Model Ensemble (NMME) project with real-time seasonal forecasts provided since 2021. This study used both historical simulations and seasonal hindcasts that are further described in the following subsections. We refer the reader to Delworth et al.[31] for further details on the specific choices made for configuration and physical parametrizations.

Historical simulations from SPEAR and CMIP6

To investigate the features of atmospheric blocking simulated by climate models, we use a 30-member ensemble of SPEAR historical simulations covering the analysis period from 1991 to 2021. Because historical simulations are available until 2014, projections following the Shared Socioeconomic Pathway 5-8.5 are appended for the period of 2015-2021. Moreover, to assess if other climate models exhibit similar atmospheric blocking statistics, the corresponding simulations from 19 global climate models participating in phase 6 of the Coupled Model Intercomparison Project (CMIP6) are also analyzed in this study. These models are chosen based on the availability of daily output from the future projection scenario (e.g., ref. 19; Table S2). Model Z500 has been uniformly regridded to a 1.25° × 1.25° horizontal resolution using bilinear interpolation to facilitate a direct comparison with ERA5 reanalysis and reduce computational costs.

SPEAR hindcasts

To investigate the predictability of atmospheric blocking, this study utilizes SPEAR hindcasts for the analysis period spanning from 1991 to 2021. Specifically, on the first day of each month, 15 ensemble members of SPEAR hindcasts are generated by inputting different initial conditions for each member, followed by a 12-month model integration. The initial conditions for the atmosphere, land, and sea ice components are obtained from a 5-member set of SPEAR restoring simulations. In these simulations, the atmospheric temperature, winds, and moisture are nudged toward the Climate Forecast System Reanalysis (CFSR) data[71], while the SSTs are restored to the Optimum Interpolation Sea Surface Temperature version 2[72]. The 5-member initial conditions of atmosphere, land and sea ice are repeated three times to create a total of 15 members. Oceanic initial conditions are derived from 15 ensemble members generated by an ocean data assimilation system coupled to the SPEAR model. This system implements a bias correction scheme, referred to as ocean tendency adjustment, to alleviate ocean model drift. We refer the reader to Lu et al.[29] for further details on the ocean data assimilation system for SPEAR hindcasts. The daily surface air temperature, SST, horizontal winds, mean sea level pressure, geopotential height, and precipitation data are used in this study. As in historical simulations, the hindcast Z500 has been regridded to a 1.25° × 1.25° horizontal resolution. For construction of the hindcast Oceanic Niño Index, as in the NOAA-CPC Oceanic Niño Index, we applied 3-month running mean to the forecasted SST anomalies in the Niño 3.4 domain (5°N-5°S, 120°-170°W), where anomaly here is defined as a deviation from the 1991-2020 base period.

Blocking detection algorithm

This study employs the MIX index that considers both Z500 anomalies and the reversal of the Z500 meridional gradient [73], which is obtained by the following procedure. First, the daily time series of Z500 anomaly is computed by subtracting its smoothed seasonal cycle that retains the first ten harmonics of the calendar-day mean values. Next, we apply the criteria of blocking detection as in Hwang et al.[5], which entails the exceedance of four thresholds: amplitude, area, consecutiveness, and persistence. The amplitude threshold is defined for each calendar month by computing the standard deviation of daily Z500 anomalies in the 30°-80°N latitudinal band over a three-month window with the target month at the center. The daily Z500

anomaly greater than 1.3 standard deviations at each grid point is considered as a blocking candidate. These blocking candidates must occupy an area larger than $2.0 \times 10^6\ km^2$, spatially overlap within consecutive days for more than 50% of the area, and persist at least 5 days to be defined as a blocking episode. The resultant blocking from these four criteria corresponds to the blocking identified from the anomaly-based index approach. The MIX index is defined by additionally applying the criteria of the reversal gradient in Z500 (GHGN) as follows.

$$GHGN(\lambda,\phi) = \max\left[Z500(\lambda,\phi) - Z500(\lambda,\phi-\Delta\phi)\right] > 0,$$

$$\lambda_{\max} - \Delta\lambda/2 < \lambda < \lambda_{\max} + \Delta\lambda/2 \; and \; \phi_{\max} - \Delta\phi/2 < \phi < \phi_{\max} + \Delta\phi/2 \quad (1)$$

where $\lambda_{\max}$ and $\phi_{\max}$ denote longitudinal and latitudinal grid point of the maximum Z500 anomaly, $\Delta\lambda$ and $\Delta\phi$ correspond to 10° and 15°, respectively. Any blocking day that fails to satisfy this gradient reversal criterion is excluded from blocking index. The aforementioned four criteria of blocking detection – amplitude, area, consecutiveness, and persistence – are imposed again to guarantee seamless identification of blocking. Consequently, this MIX index provides a blocking system that retains both enhanced magnitude and a reversed meridional gradient of Z500. For the entire process of blocking identification, we employed an open-source python package, the ConTrack-Contour Tracking[74]. While showing the results from ERA5 reanalysis for the rest of the study, we also confirmed that the identified blocking from ERA5 reanalysis is in good agreement with that from the Japanese 55 years Reanalysis (JRA-55)[75]. With respect to blocking in climate models, we adapted the same blocking detection algorithm using the daily Z500 time series from each model and each ensemble member. In addition, for consistency with models that do not retain leap days, leap days are discarded after blocking systems are detected.

In the SPEAR hindcasts, prior to blocking identification, we applied a mean bias correction technique to the daily Z500 time series in order to alleviate a drift of model mean state[20,42]. For every initialization month and ensemble member, the daily Z500 is subtracted by its lead-month dependent seasonal cycle ($\widetilde{Z500}_{SPEAR}$) and then added the corresponding observed seasonal cycle back ($\widetilde{Z500}_{ERA5}$). The resultant time series is used for blocking identification. In Fig. 3B, an estimate of the global warming contribution is eliminated by additionally removing the ensemble-mean daily Z500 anomalies of SPEAR historical simulations from the daily Z500 time series of SPEAR hindcasts prior to blocking identification.

Prediction skill analysis

To analyze how skillful SPEAR can predict the seasonal blocking frequency, we evaluate performance with the anomaly correlation coefficient (ACC), which measures a linear relationship in anomalous blocking frequency between observation and hindcasts. This metric is often used for assessing model ability to capture the observed interannual variability of the targeted variable. As in Tseng et al.[32], the ACC is computed as follows:

$$r_{xy} = \frac{\sum_{i=1}^{n}(x_i-\bar{x})(y_i-\bar{y})}{\sqrt{\sum_{i=1}^{n}(x_i-\bar{x})^2}\sqrt{\sum_{i=1}^{n}(y_i-\bar{y})^2}} \quad (2)$$

where x_i and y_i denote the seasonal blocking frequency at each grid point from SPEAR and ERA5, respectively, in the year index i. $\bar{x}$ and $\bar{y}$ denote the climatological mean blocking frequency for the 30-year period, and n denotes the total number of years, thus 30. As a rule of thumb, an ACC larger than 0.4 is generally acceptable as a skillful seasonal prediction. In addition, Spearman's rank correlation has been employed as another skill metric to ensure the robustness of the results. This non-parametric correlation estimates the monotonic relationship based on ranked blocking frequency between observation and hindcasts.

A hybrid dynamical-statistical model

We use a hybrid dynamical-statistical model to examine if a multivariate linear regression model can provide skillful prediction for longer lead times. The premise behind this approach is the potential that the model may be more skillful in predicting the large-scale precursors of atmospheric blocking than blocking itself. Previous blocking studies showed that ENSO significantly modulates the seasonal blocking frequency through its impact on extratropical circulation[24,27,76] and that latent heating located upstream of blocking plays an important role in triggering blocking onset and amplifying the ridge[49,50,77]. Along this line, two predictors from the hindcasts are chosen to construct this hybrid model: (1) Oceanic Niño Index (SST anomaly averaged from 5°S–5°N/120°–170°W) as a metric of ENSO variability and (2) precipitation over the Okhotsk Sea (50°–70°N/135°–165°E) as an estimate of the latent heating upstream of NP blocking (40°–80°N/150°E–150°W). For the latter, the choice of the domain is justified by the regression between blocking frequency and precipitation where significant positive regression coefficients are pronounced (Fig. S4). SPEAR hindcasts at lead 0 month (i.e., December 1st initialization) reproduces the observed regression pattern remarkably well (Fig. S4B, C). This upstream precipitation signal is robustly found when regressed against different domains of NP blocking frequency. The resultant hybrid model that utilizes the relationship between blocking frequency and these thermodynamic variables is written as follows:

$$block_{hybrid,m} = a_{nino34}\, x_{fc\_nino34,m} + b_{precip}\, x_{fc\_precip,m} + c_{offset}$$

The regression coefficients a_{nino34}, b_{precip}, and c_{offset} at each grid point are derived by regressing the linearly detrended DJF-mean ONI and upstream precipitation values from the ensemble-mean SPEAR hindcast at lead 0 month onto the observed NP blocking frequency (i.e., area-averaged blocking frequency from 40°–80°N/150°E–150°W). The dependence between the two predictors is removed by using their linear regression prior to be inputted to this hybrid model. To determine if the regional precipitation used in this regression model acts as a statistically significant predictor, we performed the F-test by evaluating the F-ratio (e.g., ref. 78) and found that the addition of upstream precipitation as the second predictor is statistically significant at the 5% level. Furthermore, to avoid overfitting, we applied leave-one-year-out cross-validation with the hindcast data (e.g., ref. 54) for each year in the analyzed period (i.e., 91/92-20/21 DJF) when deriving the regression coefficients. Therefore, the predictions for year y were constructed with regression coefficients calculated from all years excluding year y. Next, we input the linearly detrended DJF-mean Niño 3.4 and upstream precipitation from the ensemble-mean SPEAR hindcast at lead month m, denoted by $x_{fc\_nino34,m}$ and $x_{fc\_precip,m}$, respectively, to obtain the seasonal blocking frequency from the hybrid model, $block_{hybrid,m}$. The linear trends in the predictors are removed to exclude the potential influence of global warming trends, but the results are nearly the same if these trends are retained. Lastly, we tested different domains of upstream precipitation for the hybrid model and found qualitatively consistent results.

Data availability

The ERA5 reanalysis hourly data used in this study can be downloaded from https://cds.climate.copernicus.eu/cdsapp#!/dataset/reanalysis-era5-pressure-levels?tab=form for pressure levels and https://cds.climate.copernicus.eu/cdsapp#!/dataset/reanalysis-era5-single-levels?tab=form for single levels. The ERSSTv5 sea surface temperature dataset is available from https://psl.noaa.gov/data/gridded/data.noaa.ersst.v5.html. SPEAR Large ensemble data can be downloaded from GFDL's ftp server (https://www.gfdl.noaa.gov/spear_large_ensembles/) and seasonal retrospective forecasts data can be accessed from the NMME website (https://www.cpc.ncep.noaa.gov/products/NMME/).

Code availability

The blocking identification code used in this study is a python open-source package, CONTRACK, which is accessible from https://github.com/

steidani/ConTrack[74]. Other python custom codes are direct implementations of standard methods and statistical techniques that are described in the Methods section. These codes are available from the corresponding author upon reasonable request.

Received: 10 April 2024; Accepted: 9 September 2024;
Published online: 30 September 2024

References

1. Nakamura, N. & Huang, C. S. Y. Atmospheric blocking as a traffic jam in the jet stream. *Science* **361**, 42–47 (2018).
2. Woollings, T. et al. Blocking and its response to climate change. *Curr. Clim. Change Rep.* **4**, 287–300 (2018).
3. Seneviratne, S. I. et al. in *Climate Change 2021: The Physical Science* Basis (eds V. Masson-Delmotte et al.) 1513–1766 (Cambridge University Press, 2021).
4. Takaya, K. & Nakamura, H. Mechanisms of intraseasonal amplification of the cold Siberian high. *J. Atmos. Sci.* **62**, 4423–4440 (2005).
5. Hwang, J., Son, S.-W., Martineau, P. & Barriopedro, D. Impact of winter blocking on surface air temperature in East Asia: Ural versus Okhotsk blocking. *Clim. Dyn.* **59**, 2197–2212 (2022).
6. Yao, Y., Luo, D., Dai, A. & Simmonds, I. Increased quasi stationarity and persistence of winter ural blocking and Eurasian extreme cold events in response to Arctic warming. Part I: insights from observational analyses. *J. Clim.* **30**, 3549–3568 (2017).
7. Carrera, M. L., Higgins, R. W. & Kousky, V. E. Downstream weather impacts associated with atmospheric blocking over the Northeast Pacific. *J. Clim.* **17**, 4823–4839 (2004).
8. Luo, B., Luo, D., Dai, A., Simmonds, I. & Wu, L. Combined influences on North American winter air temperature variability from North Pacific blocking and the North Atlantic Oscillation: subseasonal and interannual time scales. *J. Clim.* **33**, 7101–7123 (2020).
9. Jeong, D. I., Yu, B. & Cannon, A. J. Links between atmospheric blocking and North American winter cold spells in two generations of Canadian Earth System Model large ensembles. *Clim. Dyn.* **57**, 2217–2231 (2021).
10. Pfahl, S. & Wernli, H. Quantifying the relevance of atmospheric blocking for co-located temperature extremes in the Northern Hemisphere on (sub-)daily time scales. *Geophys. Res. Lett.* **39**. https://doi.org/10.1029/2012gl052261 (2012).
11. Brunner, L., Schaller, N., Anstey, J., Sillmann, J. & Steiner, A. K. Dependence of present and future european temperature extremes on the location of atmospheric blocking. *Geophys. Res. Lett.* **45**, 6311–6320 (2018).
12. Ferranti, L., Magnusson, L., Vitart, F. & Richardson, D. S. How far in advance can we predict changes in large-scale flow leading to severe cold conditions over Europe? *Q. J. R. Meteorol. Soc.* **144**, 1788–1802 (2018).
13. Kautz, L.-A. et al. Atmospheric blocking and weather extremes over the Euro-Atlantic sector—a review. *Weather Clim. Dyn.* **3**, 305–336 (2022).
14. White, R. H. et al. The unprecedented Pacific Northwest heatwave of June 2021. *Nat. Commun.* **14**, 727 (2023).
15. Tibaldi, S., Tosi, E., Navarra, A. & Pedulli, L. Northern and Southern Hemisphere seasonal variability of blocking frequency and predictability. *Mon. Weather Rev.* **122**, 1971–2003 (1994).
16. Pelly, J. L. & Hoskins, B. J. How well does the ECMWF ensemble prediction system predict blocking? *Q. J. R. Meteorol. Soc.* **129**, 1683–1702 (2003).
17. Dunn-Sigouin, E. & Son, S. W. Northern Hemisphere blocking frequency and duration in the CMIP5 models. *J. Geophys. Res.: Atmos.* **118**, 1179–1188 (2013).
18. Masato, G., Hoskins, B. J. & Woollings, T. Winter and Summer Northern Hemisphere blocking in CMIP5 models. *J. Clim.* **26**, 7044–7059 (2013).
19. Davini, P. & D'Andrea, F. From CMIP3 to CMIP6: Northern Hemisphere Atmospheric blocking simulation in present and future climate. *J. Clim.* **33**, 10021–10038 (2020).
20. Athanasiadis, P. J. et al. Decadal predictability of North Atlantic blocking and the NAO. *npj Clim. Atmos. Sci.* **3**. https://doi.org/10.1038/s41612-020-0120-6 (2020).
21. Davini, P. et al. The representation of winter Northern Hemisphere atmospheric blocking in ECMWF seasonal prediction systems. *Q. J. R. Meteorol. Soc.* **147**, 1344–1363 (2021).
22. Pepler, A. S., Díaz, L. B., Prodhomme, C., Doblas-Reyes, F. J. & Kumar, A. The ability of a multi-model seasonal forecasting ensemble to forecast the frequency of warm, cold and wet extremes. *Weather Clim. Extremes* **9**, 68–77 (2015).
23. Jia, L. et al. Seasonal prediction of North American wintertime cold extremes in the GFDL SPEAR forecast system. *Clim. Dyn.* **61**, 1769–1781 (2023).
24. McKenna, M. & Karamperidou, C. The impacts of El Niño diversity on Northern Hemisphere Atmospheric Blocking. *Geophys. Res. Lett.* **50**. https://doi.org/10.1029/2023gl104284 (2023).
25. L'Heureux, M. L. et al. Observing and predicting the 2015/16 El Niño. *Bull. Am. Meteorol. Soc.* **98**, 1363–1382 (2017).
26. Nakamura, H., Nakamura, M. & Anderson, J. L. The role of high- and low-frequency dynamics in blocking formation. *Mon. Weather Rev.* **125**, 2074–2093 (1997).
27. Renwick, J. A. & Wallace, J. M. Relationships between North Pacific wintertime blocking, El Niño, and the PNA pattern. *Mon. Weather Rev.* **124**, 2071–2076 (1996).
28. Barnston, A. G., Tippett, M. K., Ranganathan, M. & L'Heureux, M. L. Deterministic skill of ENSO predictions from the North American Multimodel Ensemble. *Clim. Dyn.* **53**, 7215–7234 (2019).
29. Lu, F. et al. GFDL's SPEAR seasonal prediction system: initialization and ocean tendency adjustment (OTA) for coupled model predictions. *J. Adv. Modeling Earth Syst.* **12**. https://doi.org/10.1029/2020ms002149 (2020).
30. Choi, J. & Son, S.-W. Seasonal-to-decadal prediction of El Niño–Southern Oscillation and Pacific Decadal Oscillation. *npj Clim. Atmos. Sci.* **5**. https://doi.org/10.1038/s41612-022-00251-9 (2022).
31. Delworth, T. L. et al. SPEAR: The next generation GFDL modeling system for seasonal to multidecadal prediction and projection. *J. Adv. Modeling Earth Syst.* **12**. https://doi.org/10.1029/2019ms001895 (2020).
32. Tseng, K. C. et al. Are multiseasonal forecasts of atmospheric rivers possible? *Geophys. Res. Lett.* **48**. https://doi.org/10.1029/2021gl094000 (2021).
33. Johnson, N. C., Wittenberg, A. T., Rosati, A. J., Delworth, T. L. & Cooke, W. Future changes in boreal winter ENSO teleconnections in a large ensemble of high-resolution climate simulations. *Front. Clim.* **4**. https://doi.org/10.3389/fclim.2022.941055 (2022).
34. Joh, Y. et al. Stronger decadal variability of the Kuroshio Extension under simulated future climate change. *npj Clim. Atmos. Sci.* **5**. https://doi.org/10.1038/s41612-022-00285-z (2022).
35. Barriopedro, D., García-Herrera, R. & Trigo, R. M. Application of blocking diagnosis methods to General Circulation Models. Part I: a novel detection scheme. *Clim. Dyn.* **35**, 1373–1391 (2010).
36. Hansen, A. R. & Sutera, A. A comparison between planetary-wave flow regimes and blocking. *Tellus A* **45**, 281–288 (1993).
37. Miller, R. L., Lackmann, G. M. & Robinson, W. A. A new variable-threshold persistent anomaly index: Northern Hemisphere anomalies in the ERA-interim reanalysis. *Monthly Weather Rev.* **148**, 43–62 (2020).
38. Eyring, V. et al. Overview of the Coupled Model Intercomparison Project Phase 6 (CMIP6) experimental design and organization. *Geosci. Model Dev.* **9**, 1937–1958 (2016).
39. Liu, P., Reed, K. A., Garner, S. T., Zhao, M. & Zhu, Y. Blocking simulations in GFDL GCMs for CMIP5 and CMIP6. *J. Clim.* **35**, 5053–5070 (2022).

40. Narinesingh, V., Booth, J. F. & Ming, Y. Blocking and general circulation in GFDL comprehensive climate models. *J. Clim.* **35**, 3687–3703 (2022).
41. Berckmans, J., Woollings, T., Demory, M. E., Vidale, P. L. & Roberts, M. Atmospheric blocking in a high resolution climate model: influences of mean state, orography and eddy forcing. *Atmos. Sci. Lett.* **14**, 34–40 (2013).
42. Scaife, A. A., Woollings, T., Knight, J., Martin, G. & Hinton, T. Atmospheric blocking and mean biases in climate models. *J. Clim.* **23**, 6143–6152 (2010).
43. Martineau, P., Nakamura, H., Yamamoto, A. & Kosaka, Y. Baroclinic blocking. *Geophys. Res. Lett.* **49**. https://doi.org/10.1029/2022gl097791 (2022).
44. Shutts, G. J. The propagation of eddies in diffluent jetstreams: Eddy vorticity forcing of 'blocking' flow fields. *Q. J. R. Meteorol. Soc.* **109**, 737–761 (1983).
45. Luo, D., Cha, J., Zhong, L. & Dai, A. A nonlinear multiscale interaction model for atmospheric blocking: the eddy-blocking matching mechanism. *Q. J. R. Meteorological Soc.* **140**, 1785–1808 (2014).
46. Hwang, J., Martineau, P., Son, S.-W., Miyasaka, T. & Nakamura, H. The role of transient eddies in North Pacific blocking formation and its seasonality. *J. Atmos. Sci.* **77**, 2453–2470 (2020).
47. Nutter, P. A., Mullen, S. L. & Baumhefner, D. P. The impact of initial condition uncertainty on numerical simulations of blocking. *Mon. Weather Rev.* **126**, 2482–2502 (1998).
48. Qian, Y., Hsu, P. C., Murakami, H., Xiang, B. & You, L. A hybrid dynamical-statistical model for advancing subseasonal tropical cyclone prediction over the Western North Pacific. *Geophys. Res. Lett.* **47**. https://doi.org/10.1029/2020gl090095 (2020).
49. Steinfeld, D. & Pfahl, S. The role of latent heating in atmospheric blocking dynamics: a global climatology. *Clim. Dyn.* **53**, 6159–6180 (2019).
50. Neal, E., Huang, C. S. Y. & Nakamura, N. The 2021 Pacific Northwest heat wave and associated blocking: meteorology and the role of an upstream cyclone as a diabatic source of wave activity. *Geophys. Res. Lett.* **49**. https://doi.org/10.1029/2021gl097699 (2022).
51. Yao, Y. et al. Impact of Pacific blocking on the intraseasonal winter sea ice seesaw between the Bering and Okhotsk Seas. *Atmos. Res.* **300**. https://doi.org/10.1016/j.atmosres.2024.107227 (2024).
52. Pfahl, S., Schwierz, C., Croci-Maspoli, M., Grams, C. M. & Wernli, H. Importance of latent heat release in ascending air streams for atmospheric blocking. *Nat. Geosci.* **8**, 610–614 (2015).
53. Quinting, J. F. & Vitart, F. Representation of synoptic-scale rossby wave packets and blocking in the S2S Prediction Project Database. *Geophys. Res. Lett.* **46**, 1070–1078 (2019).
54. Black, J. et al. The predictors and forecast skill of Northern Hemisphere teleconnection patterns for lead times of 3–4 weeks. *Monthly Weather Rev.* **145**, 2855–2877 (2017).
55. Chen, X. & Luo, D. Arctic sea ice decline and continental cold anomalies: upstream and downstream effects of Greenland blocking. *Geophys. Res. Lett.* **44**, 3411–3419 (2017).
56. Cohen, J. et al. Divergent consensuses on Arctic amplification influence on midlatitude severe winter weather. *Nat. Clim. Change* **10**, 20–29 (2020).
57. Song, Y., Yao, Y., Luo, D. & Li, Y. Loss of autumn Kara-East Siberian Sea ice intensifies winter Ural blocking and cold anomalies in high latitudes of Eurasia. *Atmos. Res.* **295**. https://doi.org/10.1016/j.atmosres.2023.107038 (2023).
58. Risbey, J. S. et al. Standard assessments of climate forecast skill can be misleading. *Nat. Commun.* **12**, 4346 (2021).
59. Kirtman, B. P. et al. The North American multimodel ensemble: phase-1 seasonal-to-interannual prediction; phase-2 toward developing intraseasonal prediction. *Bull. Am. Meteorol. Soc.* **95**, 585–601 (2014).
60. Chen, L.-C., van den Dool, H., Becker, E. & Zhang, Q. ENSO precipitation and temperature forecasts in the North American multimodel ensemble: composite analysis and validation. *J. Clim.* **30**, 1103–1125 (2017).
61. Chen, R., Simpson, I. R., Deser, C. & Wang, B. Model biases in the simulation of the springtime North Pacific ENSO teleconnection. *J. Clim.* **33**, 9985–10002 (2020).
62. Kleiner, N., Chan, P. W., Wang, L., Ma, D. & Kuang, Z. Effects of climate model mean-state bias on blocking underestimation. *Geophys. Res. Lett.* **48**. https://doi.org/10.1029/2021gl094129 (2021).
63. Scaife, A. A. et al. Improved Atlantic winter blocking in a climate model. *Geophys. Res. Lett.* **38**, (2011).
64. O'Reilly, C. H., Minobe, S. & Kuwano-Yoshida, A. The influence of the Gulf Stream on wintertime European blocking. *Clim. Dyn.* **47**, 1545–1567 (2015).
65. Athanasiadis, P. J. et al. Mitigating climate biases in the midlatitude North Atlantic by increasing model resolution: SST gradients and their relation to blocking and the jet. *J. Clim.* **35**, 6985–7006 (2022).
66. Pithan, F., Shepherd, T. G., Zappa, G. & Sandu, I. Climate model biases in jet streams, blocking and storm tracks resulting from missing orographic drag. *Geophys. Res. Lett.* **43**, 7231–7240 (2016).
67. Maddison, J. W., Gray, S. L., Martinez-Alvarado, O. & Williams, K. D. Impact of model upgrades on diabatic processes in extratropical cyclones and downstream forecast evolution. *Q. J. R. Meteorol. Soc.* **146**, 1322–1350 (2020).
68. Park, M. & Lee, S. Is the stationary wave bias in CMIP5 simulations driven by latent heating biases? *Geophys. Res. Lett.* **48**. https://doi.org/10.1029/2020gl091678 (2021).
69. Pascale, S. et al. Weakening of the North American monsoon with global warming. *Nat. Clim. Change* **7**, 806–812 (2017).
70. Hersbach, H. et al. The ERA5 global reanalysis. *Q. J. R. Meteorol. Soc.* **146**, 1999–2049 (2020).
71. Saha, S. et al. The NCEP climate forecast system reanalysis. *Bull. Am. Meteorol. Soc.* **91**, 1015–1058 (2010).
72. Reynolds, R. W., Rayner, N. A., Smith, T. M., Stokes, D. C. & Wang, W. An improved in situ and satellite SST analysis for climate. *J. Clim.* **15**, 1609–1625 (2002).
73. Dunn-Sigouin, E., Son, S.-W. & Lin, H. Evaluation of Northern Hemisphere blocking climatology in the global environment multiscale model. *Mon. Weather Rev.* **141**, 707–727 (2013).
74. ConTrack: ConTrack v0.3.0 (https://zenodo.org/records/4765560, 2020).
75. Kobayashi, S. et al. The JRA-55 reanalysis: general specifications and basic characteristics. *J. Meteorol. Soc. Jpn. Ser. II* **93**, 5–48 (2015).
76. Henderson, S. A. & Maloney, E. D. The Impact of the Madden–Julian oscillation on high-latitude winter blocking during El Niño–Southern oscillation events. *J. Clim.* **31**, 5293–5318 (2018).
77. Steinfeld, D., Sprenger, M., Beyerle, U. & Pfahl, S. Response of moist and dry processes in atmospheric blocking to climate change. *Environ. Res. Lett.* **17**. https://doi.org/10.1088/1748-9326/ac81af (2022).
78. Johnson, N. C., L'Heureux, M. L., Chang, C. H. & Hu, Z. Z. On the delayed coupling between ocean and atmosphere in recent weak El Niño episodes. *Geophys. Res. Lett.* **46**, 11416–11425 (2019).
79. Bretherton, C. S., Widmann, M., Dymnikov, V. P., Wallace, J. M. & Bladé, I. The effective number of spatial degrees of freedom of a time-varying field. *J. Clim.* **12**, 1990–2009 (1999).

Acknowledgements

The authors thank Drs. Baoqiang Xiang and Bor-Ting Jong for helpful comments on an earlier version of the manuscript. The authors also acknowledge two anonymous reviewers for their constructive comments to improve the manuscript. This research is supported by award NA18OAR4320123, NA22OAR4050663D, and NA23OAR4320198 under Cooperative Institute for Modeling the Earth System (CIMES) at Princeton University and the National Oceanic and Atmospheric Administration, U.S. Department of Commerce.

Author contributions

M.P. and N.C.J. conceived the study. M.P. collected the data, performed the analyses, and wrote the manuscript with contributions from N.C.J. All authors (M.P., N.C.J., J.H., and L.J.) contributed to interpreting the results and reviewed the manuscript.

Competing interests

The authors declare no competing interests.

Additional information

Supplementary information The online version contains supplementary material available at https://doi.org/10.1038/s41612-024-00767-2.

Correspondence and requests for materials should be addressed to Mingyu Park.